Topographically induced hierarchical assembly and geometrical transformation of focal conic domain arrays in smectic liquid crystals

Apiradee Honglawan[a,1], Daniel A. Beller[b,1], Marcello Cavallaro, Jr.[a], Randall D. Kamien[b,2], Kathleen J. Stebe[a], and Shu Yang[a,c,2]

Departments of [a]Chemical and Biomolecular Engineering, [b]Physics and Astronomy, and [c]Materials Science and Engineering, University of Pennsylvania, Philadelphia, PA 19104

Edited by Noel A. Clark, University of Colorado, Boulder, CO, and approved November 2, 2012 (received for review August 24, 2012)

Controlling topological defects in 3D liquid crystal phases is a crucial element in the development of novel devices, from blue-phase displays to passive biochemical sensors. However, it remains challenging to realize the 3D topological conditions necessary to robustly and arbitrarily direct the formation of defects. Here, using a series of short pillar arrays as topological templates, we demonstrate the hierarchical assembly of focal conic domains (FCDs) in smectic-A liquid crystals that break the underlying symmetry of the pillar lattice, exhibit tunable eccentricity, and together develop a nontrivial yet organized array of defects. The key to our approach lies in the selection of the appropriate ratio of the size of focal domain to the dimension of pillars such that the system favors the "pinning" of FCD centers near pillar edges while avoiding the opposing effect of confinement. Our study unequivocally shows that the arrangement of FCDs is strongly influenced by the height and shape of the pillars, a feature that promotes both a variety of nontrivial self-assembled lattice types and the attraction of FCD centers to pillar edges, especially at regions of high curvature. Finally, we propose a geometric model to reconstruct the smectic layer structure in the gaps between neighboring FCDs to estimate the energetic effects of nonzero eccentricity and assess their thermodynamic stability.

topography | pattern | microposts | alignment

Liquid crystals (LCs) are anisotropic materials with physical properties that depend sensitively on both global and local molecular alignment. In LCs, average local molecular orientations assume geometries that can be controlled by boundary conditions (1, 2) and external fields (3, 4), and the resulting mechanical and electric anisotropies of LCs provide powerful tools in controlling the propagation of light and the assembly of soft materials (5–10). A quintessential example is the blue-phase LC organized around a 3D disclination network (11, 12); as a display component, it offers rapid response time without surface alignment (13). The ability to tailor LCs with complex, topologically structured geometries will be necessary for the next generation of display technologies and beyond.

Under appropriate boundary conditions, the smectic-A (SmA) LC phase develops a regular array of micrometer-scale defect structures known as focal conic domains (FCDs), which have gone from mere geometric curiosities to the focus of much attention in recent years as an enabling technological tool (14–17). The smectic layers in each FCD form concentric sections of Dupin cyclides, generalizations of tori, with two linear focal sets (centers of curvature), an ellipse and a confocal hyperbola (18). Whereas FCDs arise as the prototypical, kinetically trapped texture in bulk, a 2D lattice of axially symmetric toric FCDs (TFCDs) can be robustly produced in thin smectic films with antagonistic boundary conditions at the substrate and air interfaces. These TFCD arrays have been used to fabricate functional surfaces (19, 20), to direct the self-assembly of soft microsystems (17, 21, 22), to template lithographic patterns (23), and to enhance charge transport in photovoltaics and transistors (24). So far, most attention has been devoted to the precise manipulation of the locations of FCDs in 2D lattices by confining individual domains within small regions through both chemical and topographical patterning of the substrate (14, 15, 25). For device applications, it is desirable to produce FCDs with prescribed arrangements in 2D and 3D over large regions and to scale down the LC patterning. Recently, we have demonstrated epitaxial assembly of a TFCD lattice with tailored domain size and symmetry using polymer-based micropillar arrays (26).

Here, we present a unique level of control to direct the growth of FCD arrays by inducing hierarchical assembly of multiple FCDs centered at the edges of micropillars with nonoverlapping elliptical focal curves. Below a critical pillar height, the confining effects produced by anchoring conditions on the pillar sides are diminished, but the LC elastic and surface energies remain sensitive to the positions of the FCDs on the patterned substrate. Consequently, multiple FCDs "share" a single pillar and self-assemble in a hierarchical manner; changing the shape of the pillars promotes a variety of nontrivial FCD arrangements. We use a simple energetic model for the smectic LC that predicts the transition between this hierarchical assembly and topographic confinement of FCDs as the pillar height varies. Additionally, we exploit the size and spacing of the pillar array to tune the eccentricity, e, of the FCDs (see description in *SI Text*). In the case of TFCDs with circular focal curves, $e = 0$, whereas parabolic FCDs have $e = 1$. The ability to tune the eccentricity allows the creation of a versatile assortment of asymmetric FCD arrays, the first step toward the formation of 3D networks and more complex geometries. Finally, we present a geometric ansatz for the layer configurations that allows us to numerically investigate the energetic effects of nonzero eccentricity. These calculations are consistent with the observed nonzero eccentricity in the samples.

Results and Discussion

In a thin film geometry, smectic layers spontaneously assemble into FCDs in response to antagonistic boundary conditions, with homeotropic anchoring at the air interface and degenerate planar anchoring at substrate, in our system composed of the polymer SU-8. The total free energy of the system becomes a sum of three terms, the elastic energy of the LC and surface energies at both

Author contributions: R.D.K., K.J.S., and S.Y. designed research; A.H., D.A.B., and M.C. performed research; A.H., D.A.B., M.C., R.D.K., K.J.S., and S.Y. analyzed data; and A.H., D.A.B., M.C., R.D.K., K.J.S., and S.Y. wrote the paper.

The authors declare no conflict of interest.

This article is a PNAS Direct Submission.

See Commentary on page 5.

[1]A.H. and D.A.B. contributed equally to this work.

[2]To whom correspondence may be addressed. E-mail: shuyang@seas.upenn.edu or kamien@physics.upenn.edu.

This article contains supporting information online at www.pnas.org/lookup/suppl/doi:10.1073/pnas.1214708109/-/DCSupplemental.

the air and substrate interfaces: $\Delta F = \Delta F_{el} + \Delta F_{air} + \Delta F_{subs}$, where ΔF_{subs} is highly dependent on topography of the substrate and we measure the free energy with respect to horizontal flat layers. Previously, we used circular micropillar arrays of SU-8 to confine SmA LCs both by limiting the surface area on the substrate available to each FCD with degenerate planar anchoring and by imposing frustrating degenerate planar anchoring conditions along the vertical pillar sides (26). It is natural to ask (*i*) how the FCD arrangement changes when the pillars become short enough so that their vertical sides do not present an insurmountable barrier to local FCD anchoring, and (*ii*) how the arrangement of FCDs and the smectic layer structure depend on pillar shapes and lateral dimensions. Previous research on nematic LCs in micropillar arrays has highlighted the importance of pillar shape in determining the texture and controlling the placement of defects, demonstrating an inherently bistable LC display (27, 28).

Here, we fabricated three sets of short ($H = 1$ μm height) SU-8 micropillar arrays of differing cross-section (circular vs. elliptical; Fig. 1 *A1–C3*). The SmA LC film thickness cast on pillars was kept constant ($h \sim 7$ μm) so that $h\text{-}H > h_c \sim 1.5$ μm, the minimum film thickness at which FCDs form. In the case of circular pillars, the center-to-center spacing between pillars along a diagonal of the square lattice is $S = 12$ μm, roughly twice the TFCD diameter (7.2 μm) that minimizes the free energy of a single TFCD on a substrate with degenerate planar anchoring at the same h. As seen in Fig. 1 *A2* and *A3*, four FCDs formed on each pillar with their centers lying on the lattice diagonal and near the pillar edges. On elliptical pillars, the number of FCDs on each pillar decreased from four, to three ($A/B = 1.2$; Fig. 1 *B2* and *B3*), to two ($A/B = 2.5$; Fig. 1 *C2* and *C3*), which is in sharp contrast to our previously reported confinement effect with taller pillars ($H \geq 1.5$ μm) (26), where FCD centers were positioned only in the centers of pillars or evenly spaced between neighboring pillars

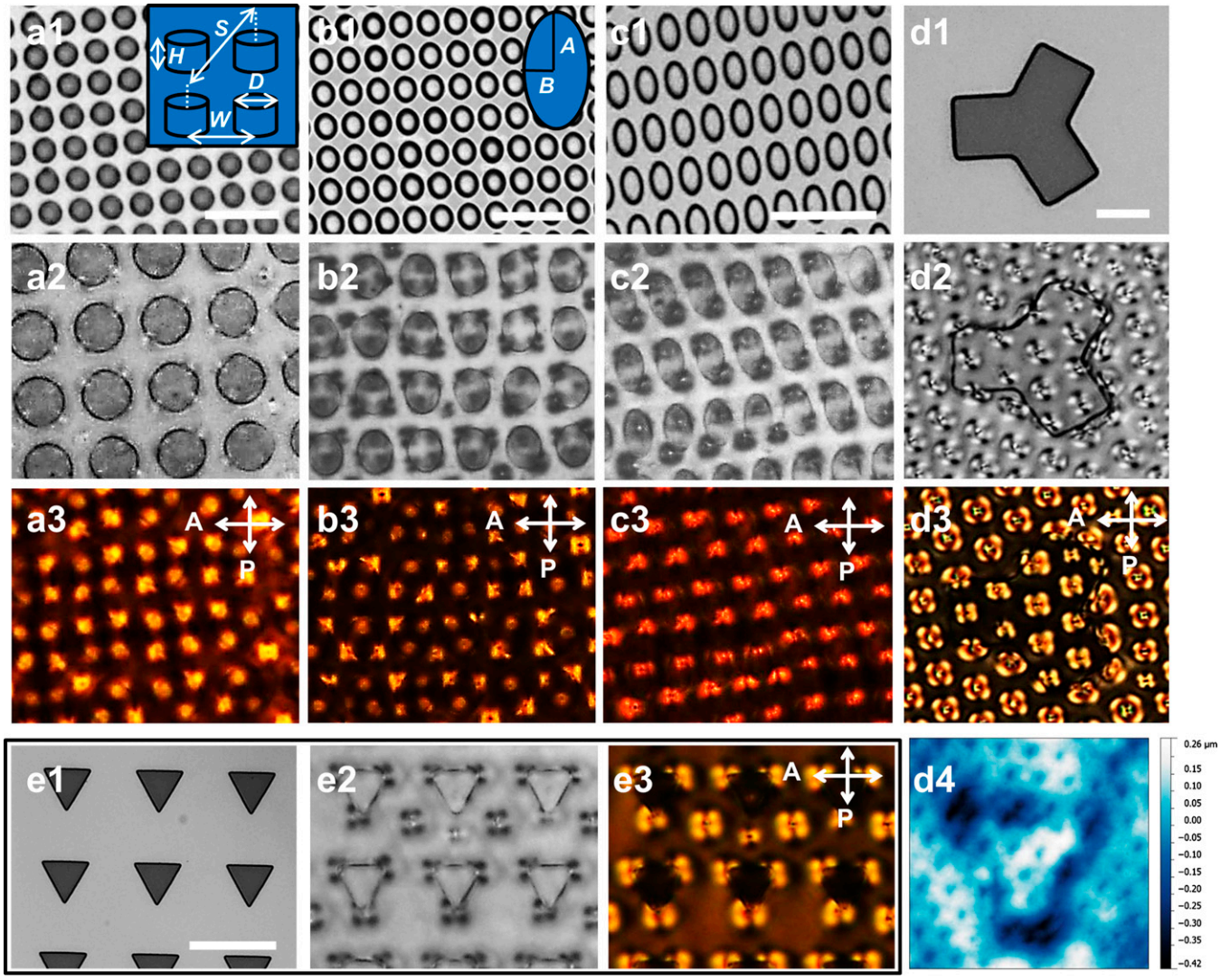

Fig. 1. (*A–E*) Formation of FCD arrays on 1-μm-tall SU-8 pillars with variable sizes and shapes. Optical images of top view of SU-8 pillars (*A1–E1*) and LC defect textures on pillars without (*A2–E2*), and with crossed polarizers (*A3–E3*). (Scale bars: 20 μm.) (*A*) Circular pillars with diameter $D = 5.5$ μm, the center-to-center spacing of the nearest pillars $W = 8.5$ μm, and the diagonal center-to-center distance of the next-nearest pillars $S = 12.0$ μm. (*B*) Elliptically shaped pillars with major axis length $2A = 6.2$ μm, minor axis length $2B = 5.2$ μm, $W = 7.4$ μm (along the shorter lattice vector), and $S = 12.2$ μm. (*C*) Elliptically shaped pillars with $2A = 7.0$ μm, $2B = 3.4$ μm, $W = 6.3$ μm (along the shorter lattice vector) and $S = 11.8$ μm. (*D*) Y-shaped post with equal peripheral dimension of 30 μm at all sides. (*E*) Triangularly shaped pillars with each side of length 10 μm. The LC thickness h is ~7 μm (*A–C*) and ~10 μm (*D* and *E*). (*D4*) AFM height profile of LC defects assembled on a Y-shaped post with equal lateral dimensions of 30 μm.

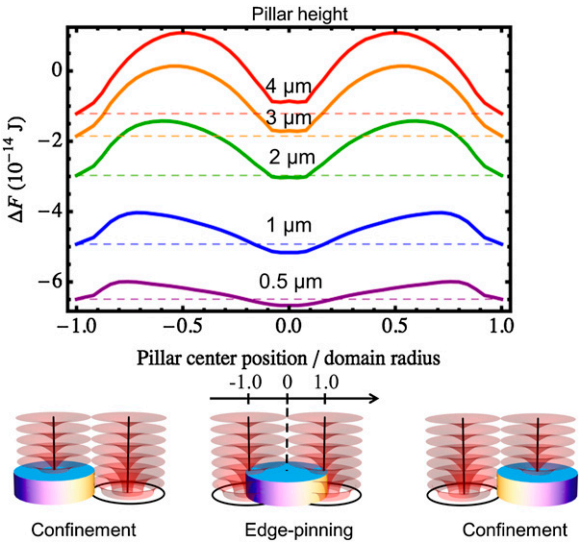

Fig. 2. A plot of the numerically calculated free energy ΔF, relative to the reference state of planar layers, as a function of the relative position of the circular pillar center along the line connecting the two TFCD centers for different pillar heights (H = 0.5–4 μm). The TFCD radius is set to 5.2 μm at LC thickness h = 10 μm on the pillar array with radius of 5.72 μm. Schematics illustrate the TFCD arrangements on the pillar with edge-pinning and confinement effects.

(see schematics in Fig. 2). Simply by reducing the height of pillars, we have effectively changed the interaction between pillar sides and FCD centers from repulsive to attractive, thereby promoting "edge-pinning" of FCD centers to the boundaries of short pillars. As the pillar's minor axis length decreases, fewer FCDs are packed with their centers on the pillar edge.

To further elucidate the edge-pinning effect, we prepared an array of 1-μm-tall, Y-shaped pillars with each side of length 30 μm, a much larger lateral scale than the cylindrical pillars. Under crossed polarizers, the Maltese cross patterns of each FCD were clearly distorted at the edges of the Y-shaped pillar (Fig. 1*D*). The distortion was even more apparent in the 3D topography of the top surface imaged by atomic force microscopy (AFM; Fig. 1*D4*): the surface was depressed at the periphery of the Y pattern but relaxed in the middle to the height of the surrounding flat region, confirming that the attraction of FCD centers to pillar edges is strong enough to disrupt the assembly of close-packed hexagonal lattices of TFCDs. The hierarchical nature of the epitaxial assembly leads to geometric relations among the orientations of FCD groups from one pillar to the next over regions spanning the whole pillar array. For example, in Fig. 1*A* the centers of the four FCDs surrounding each circular pillar form a square aligned with the substrate patterning's lattice directions consistently from pillar to pillar. Different pillar shapes yield distinct hierarchical arrangements of FCDs. An especially interesting case is presented by the most eccentric pillars in Fig. 1*C*, where the two FCDs on each pillar are connected by a line slightly rotated off the major axis of the ellipse. This pattern breaks mirror symmetry along the pillar's major axis, and the choice of ground state is consistent over regions spanning tens of pillars, even though the substrate patterning does not break this symmetry. In this way, simply by varying the pillar height and shapes, we are able to transform the arrangements of FCDs into anisotropic patterns, exhibiting order over large regions.

The importance of pillar shape to hierarchical assembly of FCDs is further evidenced by the attraction of domains to the more highly curved regions of convex pillar edges shown in Fig. 1*C*. We attribute this effect to the strong steric repulsion between the neighboring FCDs. Two FCDs will prefer to position themselves as far apart as possible while remaining tangent and keeping their centers pinned to the pillar edge. The effective attraction of FCD centers to pillar "corners" is especially evident in pillars with triangular cross-sections (Fig. 1*E*).

The transition from surface confinement to edge-pinning results from a delicate balance of the elastic (layer curvature) energy in the bulk and the surface energy of both the LC/air and the LC/substrate interfaces (*SI Text*). Degenerate planar anchoring along the pillar's vertical surface imposes an energy penalty for rod-like molecules tilted out of the vertical direction unless the molecule happens to tilt in the tangent plane to the pillar edge. For tall pillars (empirically, $H \geq 1.5$ μm), the substrate surface energy favors smectic layers horizontal at the pillar edge, a condition that is not satisfied in the interior of an FCD. Thus, the surface energy promotes confinement, with the FCD centers as far as possible from the pillar edges. In contrast, the elastic energy is concentrated most strongly near the elliptic and hyperbolic defect curves of the FCD, the focal set of the Dupin cyclides. This effect would be further enhanced by including a core energy for the defect curves; in this analysis, we have omitted this core energy because its form is uncertain and a transition from confinement to edge-pinning occurs by considering only the bulk elastic energy. If the dimension of the pillar and the LC thickness are chosen so that two or more FCDs form for each pillar, then the elastic energy often favors "hiding" the lower portion of the hyperbolic defect curve inside of the pillar, removing a significant fraction of the elastic energy (*SI Text*). The role of the pillar's top surface is more subtle, but the degenerate planar anchoring conditions on this surface generally favor the edge-pinning configuration for short pillars. The balance of these energies promotes edge-pinning as the confining effects of the pillar diminish with decreasing pillar height.

To understand the transition from confinement to edge-pinning with decreasing pillar height, we use numerical energy calculations to investigate a simplified scenario: two TFCDs and one pillar in the shape of a circular cylinder. Fig. 2 presents the calculated free energy ΔF relative to the reference state of equally spaced, horizontal planar layers, as a function of the relative position of the pillar center along the line connecting the two TFCD centers (see calculation in *SI Text*). We set the pillar radius to 1.1× the TFCD radius, so that it is possible to hide portions of both straight-line focal curves within the pillar. The LC thickness is 10 μm and the TFCD radius is 5.2 μm, chosen to minimize the analytic expression for ΔF on a flat substrate (20). For all values of H, local minima in ΔF are seen when the pillar is centered directly at the center of either TFCD, and when the pillar is positioned symmetrically between the two TFCDs. The results reveal that the global minimum changes as H decreases: for $H >$ 2 μm, the energy is minimized by centering the pillar at the center of either TFCD, corresponding to a confinement effect. For shorter pillars, the global minimum switches to a symmetric configuration of two TFCDs "sharing" a pillar equally, with their centers near the pillar edges. This calculation correctly captures the transition of FCDs from confinement to edge-pinning with decreasing pillar height.

The edge-pinning regime provides a geometric means to tune the eccentricity of FCDs. By comparing the AFM height profile of FCD arrays formed on circular and elliptical pillar arrays to LC textures observed in optical and SEM images (Fig. 3), we find two surprising features. First, the LC thickness is typically smaller over the pillar, where the substrate is raised, than over the lower regions between pillars. Along a line that passes through successive cusp-like indentations marking the terminations of hyperbolic defects at the air interface, we measure an alternating set of large and small arcs on the topmost layer. Moreover, there is a lack of axial symmetry about the cusp. The

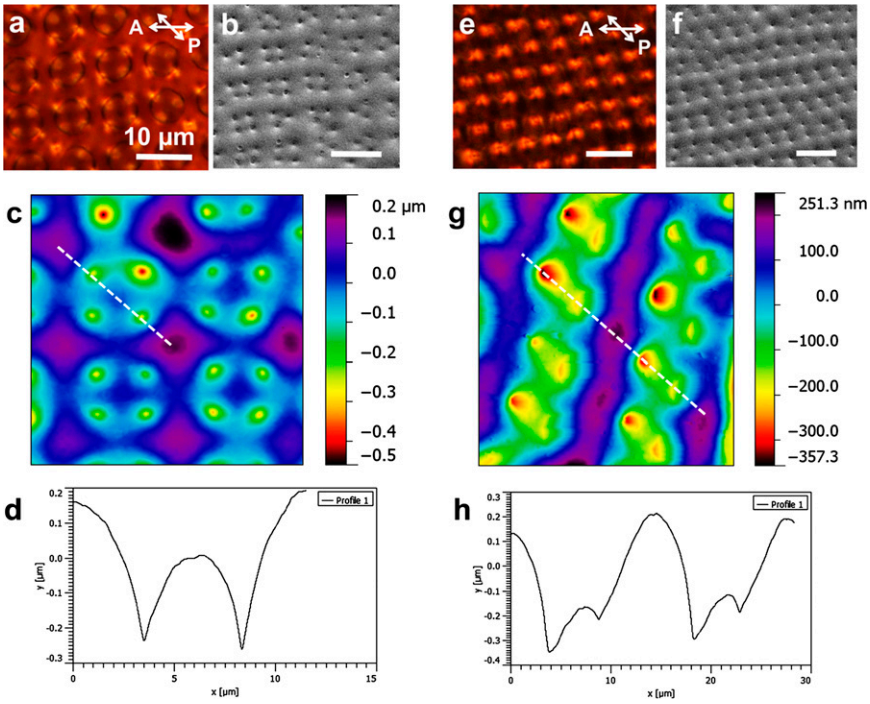

Fig. 3. Surface characterization of FCD formation on the circular (*A*–*D*) and elliptical pillar arrays (*E*–*H*); the latter corresponds to pillars seen in Fig. 1*C*. Optical images (*A* and *E*) reveal a defect texture with the polarizer and analyzer at a relative angle of 45°, and the corresponding surface topography of FCDs arrays obtained from SEM (*B* and *F*). (*C* and *G*) 3D maps of the surface of the LC films extracted from AFM measurements based on their height profiles with color representation of relative thickness of the film. (*D* and *H*) Plots of the height profiles along the dashed white lines in *C* and *G*.

absence of axial symmetry clearly implies that the edge-pinned FCDs are not toric; their eccentricity is nonzero.

FCDs with zero and nonzero eccentricity are illustrated in Fig. 4 *A*–*C*. Nontoric FCDs select a particular direction in the plane given by the direction in which the hyperbola points. In the topmost-layer profile, the periodic alternation of small and large arcs suggests the following model: the hyperbola face inward toward the pillar centers, and thus face away from each other over the space between the pillars (Fig. 4*D*).

Why should nonzero eccentricity be favored in the edge-pinning regime? We propose an answer based on geometry. Consider the square array of circular pillars (Fig. 1*A*), where S slightly exceeds 4× the pillar radius of 2.75 μm. Consequently, TFCDs in a symmetrical arrangement with their centers pinned to the edges of one pillar could not possibly have their ellipses tangent to those of the corresponding TFCDs of the neighboring pillars. A small gap would be left in between, creating extra area on the substrate with unfavorable, homeotropic anchoring rather than the preferred degenerate planar anchoring.

However, the FCD array can close the gap by shifting to small but nonzero eccentricity. Like the TFCD, an FCD of any eccentricity enjoys degenerate planar anchoring on a level surface in the area enclosed by its ellipse. Because the hyperbolic defect passes through the focus of the ellipse rather than through its center, nonzero eccentricity can shift the FCD center so that the ellipse is tangent to the ellipse of a neighboring pillar's FCD, while maintaining edge-pinning of the hyperbolic defect. Based on the dimensions presented for Fig. 1*A*, this geometric model predicts an eccentricity, $e = 0.12$, which agrees reasonably well with a separate estimate $e = 0.08$, based on the AFM data in Fig. 3 *C* and *D* (*SI Text*). Furthermore, nonzero eccentricity can decrease the elastic energy by bending the hyperbolic focal curve toward the pillar center, thus hiding more of the FCD's high-curvature central region inside the pillar.

The regular assembly of FCDs in groups of two to four poses an interesting problem as to how the LC molecules fill the interstices between the domains. For TFCDs, the interstices are filled by horizontal layers, onto which the layers of the TFCD match with continuous layer normals on a right cylinder, intersecting the circular focal curve. FCDs of nonzero eccentricity oriented in different directions cannot be joined by planar layers. Instead, elliptic-hyperbolic FCDs typically assemble in groups with their hyperbolic focal curves, or their extensions, all intersecting at a single point P, and with the elliptical focal curves tangent to their neighbors. Friedel (29) showed that FCDs associated in this way can be joined, with continuous layer position and normal direction, across bounding surfaces in the form of right circular cones with apices at P, and that include the elliptical focal curves.

It is geometrically possible for smectic layers to fill the space outside of these "corresponding cones" with portions of spheres concentric about P, again without discontinuity in layer position or normal direction, as demonstrated by Sethna and Kléman

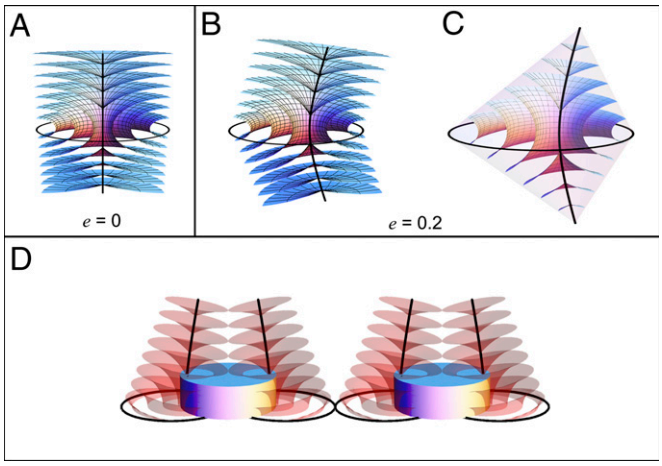

Fig. 4. Schematic illustration of internal structures of FCDs with zero (*A*) and nonzero (0.2) (*B* and *C*) eccentricity in regions bounded by a cylinder (*A* and *B*) or a cone configuration (*C*). (*D*) Representation of a possible arrangement of FCDs with nonzero eccentricity on circular pillars with the edge-pinning effect.

(30). In a model originally proposed by Bragg (31) and confirmed in experiments by Lavrentovich (32), the sample is divided into quasi-pyramidal regions, each filled by FCDs and spheres organized around a given point P, as well as wedges between the pyramids, which are filled by portions of still more FCDs. This construction fills a region entirely with layer configurations possessing only zero- and one-dimensional focal sets.

In thin-film smectics, there is no energetic prohibition of more general layer configurations with 2D focal sets outside the FCDs, provided that the focal sets of these interstitial regions lie below or above the sample as "image cusps" that are not physically realized in the smectic. In this sense, confinement dramatically expands the range of possible layer geometries even in an ideal system.

To quantitatively estimate the effect of nonzero eccentricity on the free energy, we propose an ansatz configuration for the layers in the case of four FCDs around a circular pillar as in Fig. 1*A*. (We focus on this case for modeling because it enjoys the highest symmetry.) Our ansatz employs the conical bounding surfaces of Friedel (29) but not the concentric spheres of Sethna and Kléman (30) or Bragg's pyramids (31). First, we choose a point on the hyperbolic focal curve to serve as the apex of a right circular cone C that passes through all points on the elliptical focal curve. C provides a boundary separating the FCD on the inside from some other layer configuration on the outside (Fig. 5*A*).

However, how will we bridge the gaps between the cones? Because C consists of generators for the Dupin cyclides, the layers meet the cone at right angles. Generators are straight lines consisting of surface normals to parallel layers, which remain constant from layer to layer in the normal direction and point toward the center of curvature. Consider a point E_u on the elliptical focal curve parameterized by $u \in [0,2\pi)$ (*SI Text*), and the subset of the FCD with one center of curvature at E_u, the other center lying on a variable point on the hyperbola (Fig. 5*B*). This subset consists of circular arcs concentric about E_u. Continuity of the layer normal across the bounding cone requires that the cone generator through E_u is also the generator of the layers just outside the cone. We thus choose a new center of curvature along the same generator. A natural choice is the intersection I_u of the cone generator with the corresponding generator of the neighboring FCD's bounding cone. This intersection lies somewhere below the sample. The simplest reasonable construction is to fill in the regions outside the bounding cones with circular arcs concentric about I_u, in the plane containing the cone generator through E_u and the cone normal direction along this generator.

When the construction is repeated for all $u \in [0,2\pi)$, we obtain a set of parallel surfaces that matches the FCD layers along the boundary cone and bridges the space between FCDs in a manner compatible with the observed fourfold symmetry (Fig. 5*C*). Using this construction, we can produce simulated AFM data for the topmost layer that agrees reasonably well with the experimental data (compare Figs. 5*D* and 3*C*). In combination with the structure of the FCD itself, this ansatz provides a family of space-filling smectic-layer geometries parameterized by the eccentricity. We numerically evaluate the elastic- and surface-energy integrals for these geometries and plot the total ΔF as a function of e in Fig. 5*E*. This plot shows that ΔF for eccentricity $e \lesssim 0.04$ is comparable to that at $e = 0$, whereas ΔF increases nearly monotonically for larger e. This result is consistent with the experimental observation of stability of nonzero eccentricity on the order of 0.1. Adding a core defect energy for the hyperbolic focal curve would decrease the free energy at $e \gtrsim 0.1$ relative to that at $e = 0$, due to a portion of the hyperbola disappearing inside the pillar as discussed above.

Could this system alternatively be modeled by the pyramids and wedges construction of Bragg? In the case of four FCDs around a circular pillar, we could imagine constructing an indented square pyramid around each pillar, containing four FCDs whose hyperbolas intersect at the pyramid's apex, along with portions of concentric spheres. A roughly tetrahedral wedge containing a portion of an FCD is inserted between every pair of neighboring pyramids. Finally, each four-corner meeting point of the pyramids' bases on the substrate also serves as the apex of an inverted square pyramid filled only with concave-down portions of spherical layers, forming the purple regions in Fig. 3*C*. This model predicts a concave-up region above the center of every pillar, where the layers would form portions of spheres concentric about a point above the sample. It is possible that the slight depression in the middle of the smaller arc of Fig. 3*D* is evidence of such a concave-up region. However, the concave-up region in the AFM data are no more than 1 μm in width, implying that the ellipse eccentricity exceeds 0.7, far greater than our estimate $e \sim 0.080$ based on calculations independent of our model for the interstices (*SI Text*). Furthermore, similar slight depressions are arguably visible in Fig. 3*H*, for the case of two FCDs around elliptical pillars, but are not expected in a model using Sethna and Kléman (30) filling with concentric spheres. If the bounding cones of FCDs are tangent to those of their neighbors, then the white dashed line in Fig. 3*G* passes from one FCD to the next without going through a region of spherical layers over the pillars.

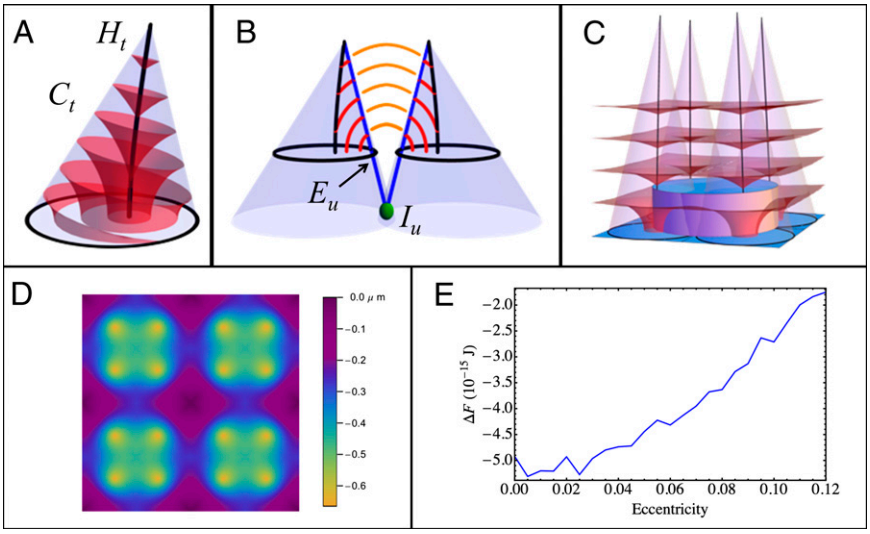

Fig. 5. Schematic illustrations of (*A*) a single FCD bounded by a cone, (*B*) a smectic layer construction bridging between two bounding cones with circular arcs concentric about I_u, in the plane containing the cone generator through E_u and the cone normal direction along this generator, and (*C*) a complete layer construction of four FCDs surrounding a pillar for all $u \in [0,2\pi)$ based on *B*. (*D*) A 2D map of topmost surface of *C* with a color representation of surface height. (*E*) A plot of total free energy of LC geometry in *C* as a function of eccentricity of FCDs.

Future studies will probe the theoretical and experimental differences between these models. With maximum parsimony in mind, we propose our model, which fits the geometry and eccentricity more readily.

In conclusion, we have shown that using SU-8 micropillar arrays of variable dimension and geometry (height, shape, and spacing) as topographical templates, we can introduce hierarchical assembly of FCDs and tune their eccentricity in a SmA LC assembly. By decreasing the micropillar height, we observe a transition from confinement of isolated domains to the hierarchical growth of FCDs, tangent to their neighbors, with their hyperbolic focal lines pinned near the pillar edges. The size and shape of the pillars can be used to control the type of hierarchical FCD arrangement; the anisotropy of the pillar shape allows us to reliably predict the locations of FCDs relative to the substrate patterning due to the effective attraction of FCDs to pillar corners. The nontrivial, but apparently smooth, matching of smectic layers between neighboring FCDs on a nonuniform substrate presents an intriguing theoretical problem for which we have suggested a geometric ansatz. These topographic tools significantly enrich the library of possible FCD arrays, making it possible to create more complex 3D structured soft systems beyond trivial assembly.

Materials and Methods

LC Synthesis. The SmA LC used in this study [4′–(5,5,6,6,7,7,8,8,9,9,10,10,11,-11,12,12,12-heptadecaflu-orododecyloxy)-biphenyl-4-carboxylic acid ethyl ester] was synthesized by a two-step reaction following the literature (33).

Fabrication of Patterned Substrates. Arrays of triangular and Y-shaped pillars with equilateral dimensions of 10 and 30 μm, respectively, were fabricated from SU-8 2010 (MicroChem Corp.) on clean silicon (Si) wafers by contact lithography using an OAI Model 200 mask aligner. SU-8 micropillars in square arrays were fabricated on Si wafers by capillary force lithography (34) (see details in *SI Text*). We use three sets of pillar arrays (Fig. 1): (*i*) a square lattice of circular pillars of diameter $D = 5.5$ μm, with pitch or center-to-center distance $W = 8.5$ μm, and corresponding diagonal pillar spacing $S = 12$ μm; (*ii*) a rectangular lattice of pillars of elliptical cross section with major axis $2A = 6.2$ μm, minor axis $2B = 5.2$ μm, pitch $W = 8.0$ μm, and diagonal pillar spacing $S = 12.2$ μm; and (*iii*) a rectangular lattice of elliptical pillars with major axis $2A = 8.5$ μm, minor axis $2B = 3.4$ μm, pitch $W = 6.3$ μm, and diagonal pillar spacing $S = 13$ μm. All pillars have the same height, $H = 1.0$ μm.

Assembly of LC Molecules on Substrates. Crystalline powders of the LC molecules were dissolved in a fluorinated solvent, Fluorinert FC-770 (3M), at a concentration of 500 mg·mL^{-1}. A 30-μL LC solution was drop-cast onto the SU-8 pillar array and heated on a Mettler FP82 hot stage with FP 90 controller to form an isotropic phase at 200 °C for 5 min; it is subsequently cooled down to 114 °C at 5 °C min^{-1} to form the SmA phase, which was quenched to room temperature.

Characterizations of LC Films. We imaged LC structures formed on various substrates by SEM on a FEI Strata DB235 focused ion beam system at 5 kV and an Olympus BX61 motorized optical microscope with crossed polarizers using CellSens software. The surface topography of the LC was characterized by a Dimension 3000 atomic force microscope (Digital Instruments) in tapping mode using open source software Gwyddion for image processing.

Calculation of Free Energy. Numerical integrations are conducted using Mathematica 7.0 and 8.0. Details of the calculations can be found in *SI Text*.

ACKNOWLEDGMENTS. We thank Elisabetta Matsumoto and Carl Modes for helpful discussions. R.D.K. thanks the Kavli Institute for Theoretical Physics (KITP) for its hospitality while this work was being completed. Support for this work was provided by National Science Foundation (NSF) Materials Research Science and Engineering Center Grant DMR11-20901, NSF Grant PHY11-25915 (to R.D.K.), an NSF Graduate Research Fellowship (to D.A.B.), and NSF Grant CMMI 09-00468.

1. Lee BW, Clark NA (2001) Alignment of liquid crystals with patterned isotropic surfaces. *Science* 291(5513):2576–2580.
2. Brake JM, Daschner MK, Luk YY, Abbott NL (2003) Biomolecular interactions at phospholipid-decorated surfaces of liquid crystals. *Science* 302(5653):2094–2097.
3. Miyajima D, et al. (2012) Ferroelectric columnar liquid crystal featuring confined polar groups within core-shell architecture. *Science* 336(6078):209–213.
4. Kang D, Maclennan JE, Clark NA, Zakhidov AA, Baughman RH (2001) Electro-optic behavior of liquid-crystal-filled silica opal photonic crystals: Effect of liquid-crystal alignment. *Phys Rev Lett* 86(18):4052–4055.
5. Smalyukh II, Lansac Y, Clark NA, Trivedi RP (2010) Three-dimensional structure and multistable optical switching of triple-twisted particle-like excitations in anisotropic fluids. *Nat Mater* 9(2):139–145.
6. Poulin P, Stark H, Lubensky TC, Weitz DA (1997) Novel colloidal interactions in anisotropic fluids. *Science* 275(5307):1770–1773.
7. Muševič I, Škarabot M, Tkalec U, Ravnik M, Žumer S (2006) Two-dimensional nematic colloidal crystals self-assembled by topological defects. *Science* 313(5789):954–958.
8. Lavrentovich OD, Lazo I, Pishnyak OP (2010) Nonlinear electrophoresis of dielectric and metal spheres in a nematic liquid crystal. *Nature* 467(7318):947–950.
9. Koenig GM, Jr., Lin IH, Abbott NL (2010) Chemoresponsive assemblies of microparticles at liquid crystalline interfaces. *Proc Natl Acad Sci USA* 107(9):3998–4003.
10. Moreno-Razo JA, Sambriski EJ, Abbott NL, Hernández-Ortiz JP, de Pablo JJ (2012) Liquid-crystal-mediated self-assembly at nanodroplet interfaces. *Nature* 485(7396):86–89.
11. Ravnik M, Alexander GP, Yeomans JM, Žumer S (2011) Three-dimensional colloidal crystals in liquid crystalline blue phases. *Proc Natl Acad Sci USA* 108(13):5188–5192.
12. Coles HJ, Pivnenko MN (2005) Liquid crystal 'blue phases' with a wide temperature range. *Nature* 436(7053):997–1000.
13. Gardiner DJ, Coles HJ (2006) Organosiloxane liquid crystals for fast-switching bistable scattering devices. *J Phys D Appl Phys* 39(23):4948–4955.
14. Ki Yoon D, et al. (2010) Organization of the polarization splay modulated smectic liquid crystal phase by topographic confinement. *Proc Natl Acad Sci USA* 107(50):21311–21315.
15. Guo W, Herminghaus S, Bahr C (2008) Controlling smectic focal conic domains by substrate patterning. *Langmuir* 24(15):8174–8180.
16. Zappone B, Lacaze E (2008) Surface-frustrated periodic textures of smectic- a liquid crystals on crystalline surfaces. *Phys Rev E Stat Nonlin Soft Matter Phys* 78(6 Pt 1):061704.
17. Yoon DK, et al. (2007) Internal structure visualization and lithographic use of periodic toroidal holes in liquid crystals. *Nat Mater* 6(11):866–870.
18. Alexander GP, Chen BGG, Matsumoto EA, Kamien RD (2010) Power of the Poincaré group: Elucidating the hidden symmetries in focal conic domains. *Phys Rev Lett* 104(25):257802.
19. Kim YH, et al. (2010) Fabrication of two-dimensional dimple and conical microlens arrays from a highly periodic toroidal-shaped liquid crystal defect array. *J Mater Chem* 20(31):6557–6561.
20. Kim YH, et al. (2009) Fabrication of a superhydrophobic surface from a smectic liquid-crystal defect array. *Adv Funct Mater* 19(18):3008–3013.
21. Pratibha R, Park W, Smalyukh II (2010) Colloidal gold nanosphere dispersions in smectic liquid crystals and thin nanoparticle-decorated smectic films. *J Appl Phys* 107(6):063511-1–063511-5.
22. Milette J, et al. (2012) Reversible long-range patterning of gold nanoparticles by smectic liquid crystals. *Soft Matter* 8(24):2593–2598.
23. Kim YH, Yoon DK, Jeong HS, Jung HT (2010) Self-assembled periodic liquid crystal defects array for soft lithographic template. *Soft Matter* 6(7):1426–1431.
24. O'Neill M, Kelly SM (2003) Liquid crystals for charge transport, luminescence, and photonics. *Adv Mater* 15(14):1135–1146.
25. Kim YH, et al. (2009) Confined self-assembly of toric focal conic domains (the effects of confined geometry on the feature size of toric focal conic domains). *Langmuir* 25(3):1685–1691.
26. Honglawan A, et al. (2011) Pillar-assisted epitaxial assembly of toric focal conic domains of smectic-a liquid crystals. *Adv Mater* 23(46):5519–5523.
27. Kitson S, Geisow A (2002) Controllable alignment of nematic liquid crystals around microscopic posts: Stabilization of multiple states. *Appl Phys Lett* 80(19):3635–3637.
28. Kitson SC, Geisow AD (2004) Bistable alignment of nematic liquid crystals around microscopic posts. *Mol Cryst Liquid Cryst* 412(1):153–161.
29. Friedel G (1922) Mesomorphic states of matter. *Ann Phys* 18:273–474. French.
30. Sethna JP, Kléman M (1982) Spheric domains in smectic liquid-crystals. *Phys Rev A* 26(5):3037–3040.
31. Bragg W (1934) Liquid crystals. *Nature* 133(3360):445–456.
32. Lavrentovich OD (1986) Hierarchy of defect structures in space filling by flexible smectic-A layers. *Sov Phys JETP* 64(5):1666–1676.
33. Percec V, Johansson G, Ungar G, Zhou J (1996) Fluorophobic effect induces the self-assembly of semifluorinated tapered monodendrons containing crown ethers into supramolecular columnar dendrimers which exhibit a homeotropic hexagonal columnar liquid crystalline phase. *J Am Chem Soc* 118(41):9855–9866.
34. Zhang Y, Lin C-T, Yang S (2010) Fabrication of hierarchical pillar arrays from thermoplastic and photosensitive SU-8. *Small* 6(6):768–775.